Validation of a Two-Phase CFD Model for Autogenous Pressurization and Expulsion

Steven Soriano*
HX5 and NASA Glenn Research Center, Cleveland, OH 44135, USA

Olga Kartuzova† and Mohammad Kassemi‡
National Center for Space Exploration Research (NCSER), Case Western Reserve University and NASA Glenn Research Center, Cleveland, OH 44135, USA

Daniel Hauser §
NASA Glenn Research Center, Cleveland, OH 44135, USA

This paper presents a two-phase computational fluid dynamics (CFD) model for simulating autogenous pressurization and expulsion in a cryogenic liquid hydrogen storage tank. The model uses a volume-of-fluid (VOF) approach combined with the kinetics-based Schrage equation to accurately capture the phase boundary and interfacial heat, mass, and momentum transfer between vapor and liquid phases. The model is validated against experimental data from NASA's K-site tank facility. Specifically, it is tested against experimental case 225, which involved autogenous pressurization and controlled expulsion of liquid hydrogen. Various turbulence models are evaluated to assess their influence on model accuracy. The CFD simulations successfully replicate key thermodynamic behaviors observed during the experiments, including pressure evolution, temperature profiles, and phase-change dynamics at the vapor-liquid interface. The predicted tank pressures and temperatures agree well with the experimental data. The pressurant mass predictions are also within 16% of the observed values. This study emphasizes the importance of selecting appropriate turbulence models to accurately simulate the complex flow and heat transfer phenomena during tank autogenous pressurization and expulsion. By improving the accuracy and reliability of CFD models for these processes, this research contributes to developing efficient cryogenic propellant management strategies for future space missions.

I. Nomenclature

E	=	Energy
$\mathbf{g}$	=	Gravity
h	=	Surface curvature
k	=	Thermal conductivity
M	=	Molar mass of fluid
p, P	=	Pressure
R	=	Gas constant
T	=	Temperature
t	=	Time
$\mathbf{v}$	=	Velocity
c_p	=	Heat capacity at constant pressure
m	=	Mass

*Mechanical Engineer, Fluid and Cryogenic Systems Branch, and AIAA Member.
†Research Assistant Professor, Department of Mechanical & Aerospace Engineering, and AIAA Member.
‡Research Professor, Department of Mechanical & Aerospace Engineering, and AIAA Associate Fellow.
§Fluids Engineer, Fluid and Cryogenic Systems Branch.

Greek

α	=	Cell value of volume fraction
ϕ	=	Face value of volume fraction
μ	=	Dynamic viscosity
ρ	=	Density
τ	=	Stress tensor
σ	=	Accommodation coefficient

Subscripts

i	=	Interface or phase
l	=	Liquid
v	=	Vapor

II. Introduction

Since the 1960s, NASA's advancements in cryogenic propellant technologies have been fundamental to enhancing spacecraft efficiency. A significant challenge in this field is managing volatile cryogenic propellants under microgravity conditions. In such environments, controlling the pressurization and expulsion processes required to transfer propellant into storage or deliver it to engines becomes increasingly complex. To address these issues, NASA Glenn Research Center and its partners have conducted extensive ground-based experiments to investigate associated challenges.

Effective management of pressurization and expulsion in cryogenic propellant tanks is critical for the reliable operation of guidance, navigation, and control systems, directly impacting mission stability and efficiency. In particular, autogenous pressurization, where the tank's own vaporized propellant is used as the pressurant, presents significant challenges. If the condensation of this vapor inside the tank is not adequately accounted for, it can lead to pressure collapse—a rapid decrease in tank pressure that may compromise the propellant flow required for stable engine or storage operation.

Understanding the behavior of cryogenic propellants during autogenous pressurization and expulsion is essential for designing modern spacecraft for upcoming NASA missions. Given the high costs of experimenting with cryogenic fluids across different gravitational conditions, NASA is developing and refining CFD models to understand better the complex heat and mass transfer dynamics. These models simulate the physical phenomena and evaluate the propellant tank's fluid dynamics and heat transfer performance. However, due to the unique thermodynamic and fluid dynamic behaviors of cryogenic propellants like liquid hydrogen, these models require rigorous validation against experimental data to ensure their reliability during operation. By validating these models through ground-based experiments, NASA aims to enhance their precision and reliability for future space applications.

Several experimental and computational studies have contributed to our understanding of pressurization and expulsion dynamics, providing critical benchmarks for CFD validation. This study builds upon these foundations, using experimental results from NASA's K-site facility to validate a two-phase CFD model for liquid hydrogen.

Hardy et al. [1] performed experimental studies to measure thermodynamic parameters during ramp pressurization of liquid and slush hydrogen in a 1.74-meter-diameter spherical tank at the K-site facility. This work provided essential data on pressurant gas requirements, system mass balances, and temperature distributions in the ullage and along the tank walls. These results form the experimental basis for the current CFD validation, offering detailed temperature and pressure data under static pressurization and expulsion conditions directly applicable to liquid hydrogen.

In a related effort, Baker et al. [2] conducted CFD validation using static pressurization and expulsion test data from the K-site dataset, focusing on liquid methane. Their study demonstrated strong agreement between CFD predictions and experimental measurements, particularly regarding pressurant mass and tank temperature profiles, and included a CFD-predicted phase-change rate. Whereas their work involved liquid methane, the current study expands upon it by applying similar methodologies to liquid hydrogen—a propellant with distinct thermodynamic behaviors requiring separate validation.

Longmire et al. [3] also validated CFD models against K-site experimental data, extending the validation scope to include non-condensable pressurants and dynamic expulsion conditions, including sloshing. Although their work addresses dynamic expulsion behaviors, the present study is focused on static pressurization and expulsion conditions, providing an additional validation case specifically for liquid hydrogen without the complexities of dynamic or sloshing

behaviors.

Recently, Kartuzova et al. [4] validated a CFD liquid hydrogen tank pressurization model and examined induced sloshing and pressure collapse. Their work, based on experiments conducted at the K-site, underscored the importance of accurate CFD simulations for cryogenic fluids under static and sloshing conditions. In contrast, this study aims to enhance CFD accuracy for static liquid hydrogen pressurization and expulsion, serving as an additional validation case for stable, non-sloshing conditions.

The current research builds on foundational studies by validating a two-phase CFD model using experimental data from autogenous liquid hydrogen pressurization and expulsion tests conducted at the K-site facility. The model incorporates the VOF method and the kinetics-based Schrage equation to accurately capture the phase boundary and interfacial heat, mass, and momentum transfer between the vapor and liquid phases. By improving the accuracy and reliability of CFD models, this research contributes to developing more efficient and effective cryogenic propellant management strategies for future space missions.

The validation process involves comparing the CFD model's predicted tank pressures, temperatures, and pressurant requirements with experimental data. The details of the CFD model, including the governing equations, boundary conditions, and numerical implementation, are thoroughly presented. The validation results are analyzed to highlight the model's strengths and identify areas for further improvement.

III. Experimental Setup

A. K-site Testing Facilities

The experiment used for this validation study was performed at NASA Plum Brook K-site facility [1]. The K-site experiment tank was a 1.74 m diameter 6061 aluminum tank mounted inside a 7.6 m diameter stainless steel vacuum chamber. The tank had an ellipsoidal shape with an internal volume of 1.75 m^3. Figures 1a and 1b show the vacuum chamber, the tank, and the schematic.

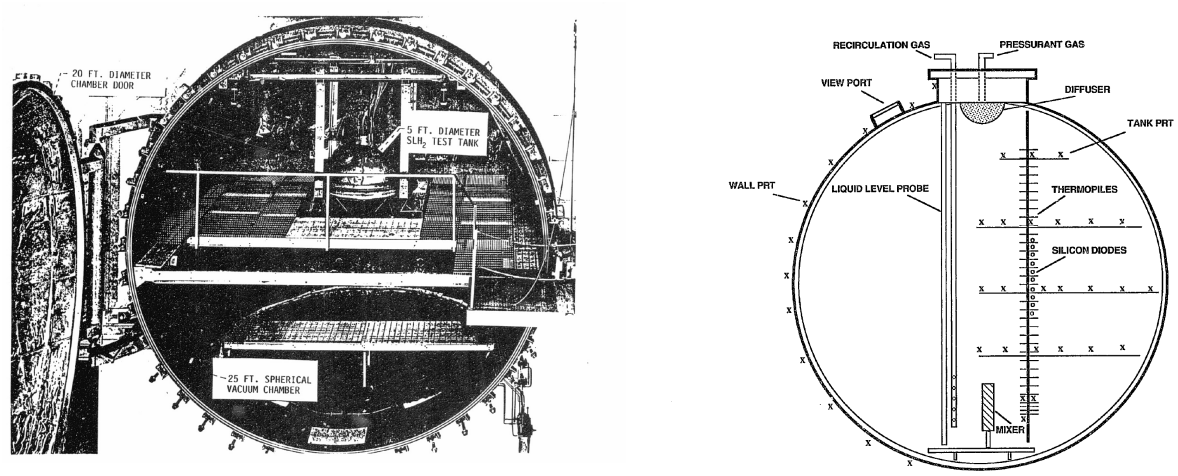

(a) K-site tank and vacuum chamber illustration. **(b) K-site tank schematic.**

Fig. 1 K-site tank and facility.

The experiment aimed to determine thermodynamic parameters during the ramp pressurization of slush hydrogen (SLH_2) and normal boiling point liquid hydrogen ($NBPH_2$) as part of the National Aero-Space Plane program. This paper, however, focuses on the experimental results using $NBPH_2$. In the tests, the tank was pressurized with gaseous hydrogen from atmospheric pressure (14.7 psia) to target pressures of 25, 35, and 50 psia. After pressurization, a hold phase followed, during which the inflow of gaseous hydrogen was reduced to maintain the target pressure for a specific duration. In the final expulsion phase, the gaseous hydrogen flow increased, enabling liquid hydrogen discharge from the tank.

The test tank instrumentation, shown in Figure 1b, included temperature diodes to monitor temperatures on the tank walls and within the tank, pressure transducers, a liquid level probe, and a mass flow meter to measure the pressurant

and expelled propellant.

B. Experimental Results

Case 225 from the experimental report was selected for validation in this study [1]. This case was an $NBPH_2$ pressurization and expulsion test with a non-constant inlet gas temperature. During the test, the inlet gas temperature increased nonlinearly over time. Initially, it was 20 K, rising gradually to 80 K by the end of the pressurization phase. The temperature remained around 80 K during the hold phase and continued to increase gradually, reaching 250 K by the end of the expulsion phase.

The tank pressure was monitored throughout the test. It showed an initial linear rise during pressurization, reaching a peak before stabilizing in the hold phase. During expulsion, the pressure was maintained at a set target level (50 psia) as liquid hydrogen was discharged from the tank.

The pressurant mass during the expulsion period was measured, showing a linear increase in pressurant over time. This steady addition of pressurant was necessary to maintain the target tank pressure as the liquid hydrogen was expelled.

Near the end of the expulsion period, the temperature distribution within the tank and along the tank wall was profiled. The temperatures increased along the tank's height, with higher temperatures observed near the top due to the warmer incoming gas. The ullage and the tank wall exhibited a slightly curved temperature profile, suggesting non-uniform heating effects and complex thermal interactions between the incoming gas, the tank structure, and liquid hydrogen.

These experimental observations provide valuable insights into the thermodynamic processes occurring during the test. Key parameters—such as the inlet gas temperature, pressure dynamics, pressurant mass requirements, and temperature distributions—are essential for validating the CFD model. Accurately capturing these trends and values in the CFD simulations will be crucial for model validation.

IV. Computational Model

A. Governing Equations

Fluid flow and heat transfer in the tank are described in terms of the continuity, Navier-Stokes, and energy equations for both phases:

$$\frac{\partial \rho}{\partial t} + \nabla(\rho \mathbf{v}) = 0, \tag{1}$$

$$\frac{\partial}{\partial t}(\rho \mathbf{v}) + \nabla(\rho \mathbf{v}\mathbf{v}) = -\nabla p + \nabla \left[\mu_{eff} \left(\nabla \mathbf{v} + \nabla \mathbf{v}^T \right) \right] + \rho \mathbf{g} + \mathbf{F}_{vol}, \tag{2}$$

$$\frac{\partial}{\partial t}(\rho E) + \nabla(\mathbf{v}(\rho E + p)) = \nabla \left(k_{eff} \nabla T \right) + S_h. \tag{3}$$

The present study treats the liquid phase as incompressible with variable temperature-dependent properties, except for density. The liquid density is allowed to vary linearly with temperature in the body force term of the momentum equation according to the Boussinesq approximation. The vapor is modeled as a compressible ideal gas. In this study, the movement of the interface is captured diffusely using the VOF method, as published by Hirt and Nichols [5]. Interfacial energy, momentum, and mass balances are applied using source terms in the diffuse interfacial region.

B. VOF Model

In the VOF method, a volume fraction is defined in each cell such that the volume fractions of all the phases sum to unity. In the cell, the change in the interface can be tracked by solving a continuity equation for the volume fraction of the q^{th} phase:

$$\frac{1}{\rho_q} \left[\frac{\partial}{\partial t} \left(\alpha_q \rho_q \right) + \nabla \cdot \left(\alpha_q \rho_q \mathbf{v}_q \right) = S_{\alpha_q} \right], \tag{4}$$

where the volume fraction for the primary phase is determined from:

$$\sum_{q=1}^{n} \alpha_q = 1. \tag{5}$$

In the VOF method, the field variables and properties are defined in terms of the volume fraction, which for a general system can be written as:

$$\rho = \sum_{q=1}^{n} \alpha_q \rho_q, \quad \mu_{eff} = \sum_{q=1}^{n} \alpha_q \mu_{eff_{q'}} \quad k_{eff} = \sum_{q=1}^{n} \alpha_q k_{eff_q}. \tag{6}$$

In this fashion, the continuity, momentum, and energy equations, as described by Eq. (1)-(3), can be solved throughout the domain for the temperatures and velocities in the two phases. In the VOF model, energy (E) and temperature (T) are treated as mass-averaged variables:

$$E = \frac{\sum_{q=1}^{n} \alpha_q \rho_q E_q}{\sum_{q=1}^{n} \alpha_q \rho_q}, \tag{7}$$

where E_q is based on the specific heat of the q^{th} phase and the shared temperature.

Evaporation and condensation at the interface are modeled as a source term in the continuity equation for the volume fraction (Eq. 4), i.e.:

$$S_{\alpha_q} = \dot{\mathbf{m}}_i \cdot \mathbf{A}_i, \tag{8}$$

where $\mathbf{A}_i$ is an interfacial area density vector, and $\dot{\mathbf{m}}_i$ is a mass flux vector, which for near equilibrium conditions can be determined based on the Schrage equation [6]:

$$|\dot{\mathbf{m}}| = \left(\frac{2\sigma}{2-\sigma}\right)\left(\frac{M}{2\pi R}\right)^{1/2}\left(\frac{P_i}{T_i^{1/2}} - \frac{P_v}{T_v^{1/2}}\right). \tag{9}$$

Here σ is the accommodation coefficient (a value of 0.001 was used for the CFD simulations); M is the molar mass of the fluid; R is the universal gas constant; P_i and P_v are, respectively, the interfacial and vapor pressures (it was assumed that $P_i \cong P_{sat}$); T_i and T_v are, respectively, the interfacial and vapor temperatures (it was assumed that $T_i = T_v \cong T_{sat}$ at the interface). Finally, $\mathbf{A}_i$ is defined as:

$$\mathbf{A}_i = |\nabla \alpha|, \tag{10}$$

where α is the volume fraction of the primary phase.

In the present implementation, the surface tension forces at the interface are modeled via the continuum surface force (CSF) model of Brackbill et al. [7]. In this model, the surface tension forces at the interface are transformed into a volume force ($\mathbf{F}_{vol}$), which is added as a source to the momentum equation:

$$\mathbf{F}_{\text{vol}} = \sum_{\text{pairs } ij, i<j} \sigma_{ij} \frac{\alpha_i \rho_i h_i \nabla \alpha_j + \alpha_j \rho_j h_j \nabla \alpha_i}{\frac{1}{2}\left(\rho_i + \rho_j\right)}, \tag{11}$$

where h_i is the surface curvature calculated from the local gradients in the surface normal at the interface:

$$h_i = \nabla \cdot \widehat{\mathbf{n}}. \tag{12}$$

V. Numerical Implementation

A computational model was developed to simulate the experimental conditions described in Section III, replicating the tank geometry, initial conditions, and operational procedures of the K-site case 225 experiment. The simulations aimed to mirror the pressurization, hold, and expulsion phases by accurately modeling the fluid dynamics and heat transfer within the tank.

All simulations were performed using ANSYS Fluent 2024 R1[8]. A custom in-house user-defined function (UDF) was developed to implement the VOF method and the kinetics-based Schrage equation for interfacial mass transfer, as

described in Section IV.B. This UDF allowed for accurate modeling of the phase boundary and associated heat, mass, and momentum transfer between the liquid and vapor phases.

A 2D axisymmetric model was employed to simplify the computational domain. The flow within the tank was simulated using a laminar, a Shear Stress Transport (SST) k-ω turbulence model [9], and an Improved Delayed Detached Eddy Simulation (IDDES) turbulence model [10] [11].

A bounded second-order time-stepping scheme with a time step size of 5×10^{-3} seconds was employed to solve the time-dependent conservation equations for both the ullage and liquid regions. Convective fluxes in the momentum, energy, and turbulence equations were discretized using a second-order upwind scheme. However, for the IDDES model, only the momentum equations were discretized using a bounded central difference method instead. Pressure-velocity coupling was achieved using the Pressure-Implicit with Splitting of Operators (PISO) method.

A. Turbulence models

Accurate prediction of mass transfer, pressure evolution, and temperature distribution within the tank requires appropriate turbulence modeling, as turbulence significantly influences mixing, heat transfer, and phase change processes. In this study, three models were employed: the laminar model, the SST k-ω model, and the IDDES model, to compare their effectiveness in capturing the flow behaviors and to assess the impact of turbulence modeling on the simulation results.

The laminar model assumes smooth and orderly fluid motion without accounting for turbulence effects. It was included in this study as a baseline to evaluate whether turbulent effects significantly influence the tank's behavior under the conditions present during pressurization and expulsion. By comparing the laminar model results with those from turbulence models, we can assess the necessity of incorporating turbulence modeling for accurate predictions.

The SST k-ω model is a two-equation eddy-viscosity turbulence model that combines the robustness of the k-ϵ model in free shear flows with the accuracy of the k-ω model in near-wall regions. This hybrid approach makes it particularly effective for flows with complex boundary layers, enabling it to accurately capture boundary layer effects and phase change processes near the liquid-gas interface.

Regarding mass transfer, the SST k-ω model affects the prediction of interfacial mass flux by influencing turbulence levels near the interface, which can enhance or suppress mixing and heat transfer across the phase boundary. However, the model requires careful treatment near the vapor-liquid interface to ensure realistic flow behavior. The SST k-ω tends to predict large turbulent kinetic energy (TKE) production at the interface, increasing turbulent viscosity levels. This can artificially enhance diffusion and impact the accuracy of mass transfer and temperature predictions. This excessive turbulence can lead to overestimating interfacial mixing and heat transfer, affecting the pressure evolution within the tank.

To mitigate this, a correction is applied in the ω equation based on the gradient of the volume fraction, increasing the dissipation term in the TKE equation. This adjustment effectively reduces turbulence levels at the interface, leading to more accurate predictions of mass transfer rates, pressure, and temperature distributions. This correction corresponds to the turbulence-damping option in Ansys Fluent [8].

This study used a turbulence damping factor of 100 for the SST k-ω model. Simulations were also conducted with damping factors ranging from 0 to 10,000 to confirm that higher values did not yield additional effects. The choice of the damping factor is crucial, as it directly influences the model's ability to predict correct turbulence levels, affecting mass transfer and thermal fields. Without an appropriate damping factor, the model may produce nonphysical results due to excessive turbulence at the interface, leading to artificially high mass transfer rates and unrealistic pressure and temperature predictions. This occurs because unmitigated turbulence enhances mixing and diffusion beyond what is physically realistic, misrepresenting the actual interfacial phenomena.

The IDDES model is a hybrid turbulence modeling approach that combines Reynolds-Averaged Navier-Stokes (RANS) and Large Eddy Simulation (LES) techniques. Designed to resolve large-scale turbulent structures while modeling smaller scales, the IDDES model dynamically transitions between RANS and LES modes based on local flow conditions, balancing accuracy and computational efficiency.

In terms of mass transfer prediction, the IDDES model's ability to capture unsteady, large-scale turbulent eddies allows for a more accurate representation of mixing processes and heat transfer across the liquid-vapor interface without artificial damping. Unlike RANS models, the IDDES model naturally adjusts turbulent kinetic energy near the interface by dynamically controlling the level of turbulence resolution. This dynamic adjustment enables the IDDES model to resolve appropriate turbulence scales that influence mass transfer, pressure evolution, and temperature distributions, potentially leading to more accurate predictions of these phenomena within the tank.

The laminar model provides a baseline to assess whether turbulence significantly affects the system under study. The SST k-ω model is widely used to balance accuracy and computational efficiency in capturing near-wall turbulence and boundary layer effects. The IDDES model, with its hybrid RANS-LES approach, offers the potential to capture unsteady and large-scale turbulent structures that may influence mass transfer and thermal fields within the tank. By comparing these models, we aim to identify the most suitable turbulence modeling approach for accurately predicting the behavior of cryogenic propellant tanks during autogenous pressurization and expulsion.

B. Tank Geometry and Computational Mesh

The CFD simulations utilized a model of the K-site tank. Figure 2a represents a 2D schematic of the tank geometry used in the simulations. In the experiment, incoming pressurant gas passed through a screen before entering the tank to ensure uniform distribution. For the CFD model, this was simplified by assuming that the gas enters the tank uniformly and perpendicular to the diffuser located at the top of the tank. A circular outlet is positioned directly beneath the gas inlet at the bottom of the tank.

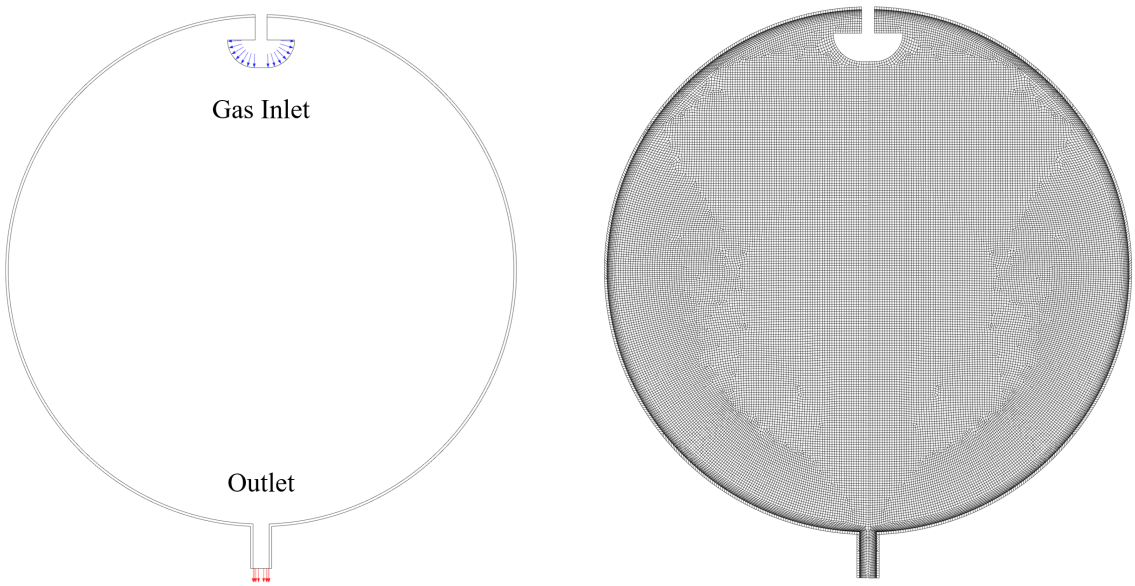

Fig. 2 (a) Tank geometry and (b) computational mesh used for CFD.

An unstructured computational mesh with an average cell size of 5 mm (21,711 cells) was generated for the simulations, as depicted in Figure 2b. Mesh refinement was applied near the tank walls to capture boundary layer effects and ensure accurate resolution of gradients in velocity and temperature.

C. Initial Conditions

To simulate the pressurization period, the initial conditions were set to match the experimental values for Case 225, as listed in Table 1. The initial tank pressure was set to 15 psia, and the initial ullage volume was set to 8.4% of the total tank volume. The liquid and vapor temperatures were initialized to the saturation temperature corresponding to the initial tank pressure.

The material properties of liquid hydrogen and its vapor were obtained from the NIST REFPROP database using the properties of parahydrogen. Material properties such as specific heat, thermal conductivity, and viscosity were allowed to vary with temperature. This approach accurately captures temperature-dependent effects on heat transfer and fluid flow.

Table 1 K-site case 225 test parameters.

Case #	Ullage Volume, %	Initial Pressure, psia	Expulsion Pressure, psia
225	8.4	15	48.9

Pressurization Time, s	Hold Time, s	Expulsion Time, s
30	30	500

D. Boundary Conditions

The CFD model incorporates conjugate heat transfer through the aluminum tank wall. Non-slip boundary conditions are applied on the inner surface of the tank wall, and the contact angle between the liquid hydrogen and the tank wall is set to 0 degrees, representing complete wetting. During the pressurization and hold stages, the outlet at the bottom of the tank is modeled as a wall to prevent fluid outflow. During the expulsion phase, the outlet is assigned a mass flow outlet boundary condition to allow the discharge of liquid hydrogen. The outlet mass flow rate during expulsion was set to match the experimental value of 0.217 kg/s. Gaseous hydrogen is injected uniformly at the gas inlet as shown in Figure 2a. The inlet gas temperature in the CFD model was set to experimental values.

For this case, transient experimental data for the inlet mass flow rate were unavailable. Instead, only the total pressurant mass added at the end of the pressurization and expulsion phases was reported. To estimate the inlet mass flow rate during pressurization, we initially divided the total added mass by the duration of the pressurization phase, yielding a constant pseudo-inlet mass flow rate. However, simulations using this estimated mass flow rate indicated that the tank did not reach the target pressure within the experimental test time.

Due to discrepancies and uncertainties in the experimental data during pressurization, we implemented a pressure inlet boundary condition to replicate the pressure ramp leading to the target pressure for expulsion. The inlet gas temperatures in the CFD simulations were kept consistent with the experimental values. During the expulsion phase, we used a proportional controller within the CFD model to maintain the tank pressure at the target level. This controller was implemented using a UDF and calculated the average tank pressure at each time step, adjusting the inlet mass flow rate according to the equation:

$$\dot{m}_{\text{in}} = \dot{m}_{\text{in, previous}} + k \left(P_{\text{set}} - P_{\text{avg}} \right) \tag{13}$$

where k is the proportional gain. In our simulations, we used a proportional gain value of $k = 0.005$, effectively controlling the tank pressure. Here, P_{set} is the target pressure, and P_{avg} is the average pressure within the tank. This UDF allowed for dynamic inlet mass flow rate adjustment, ensuring consistent tank pressure throughout the expulsion phase.

VI. Results & Discussion

CFD results were compared with experimental data. Figure 3 displays CFD and experimental tank pressure evolutions throughout the test. As outlined in Section V.D, a pressure boundary condition was implemented for the pressurization and hold phases of the simulation, addressing uncertainties in the experimental data and discrepancies observed in CFD results. A proportional controller was used to regulate the pressure in the tank during the expulsion stage, and the amount of pressurant gas required to maintain pressure was monitored.

Figure 4 presents the CFD-predicted mass transfer rate in the tank without experimental data for comparison, as these measurements were not recorded during testing. It compares mass transfer rates predicted by different turbulence models. All models show condensation occurring during the pressurization and hold stages where the vapor pressure at the interface is increasing and overcoming its saturation point. At the start of expulsion, there is an interplay between evaporation and condensation. However, condensation is prevalent throughout the expulsion. This interplay is attributed to vapor pressure increasing relative to the saturation point and hotter inlet gas reaching the interface, causing liquid at the interface to evaporate. All three models display similar trends between evaporation and condensation phases; however, the SST k-ω model predicts a greater magnitude of condensation and evaporation.

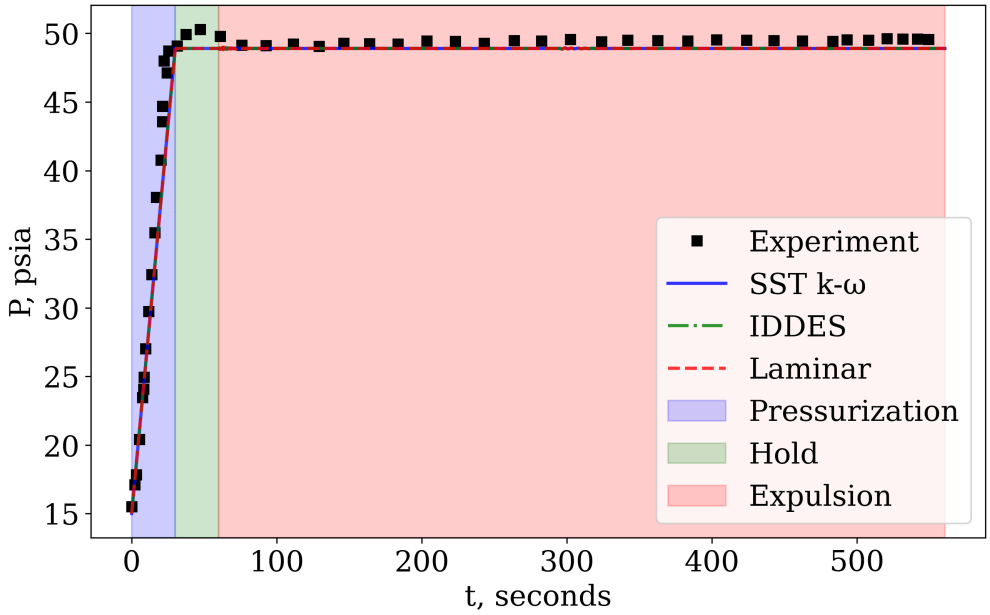

Fig. 3 CFD and experimental tank pressure during the test.

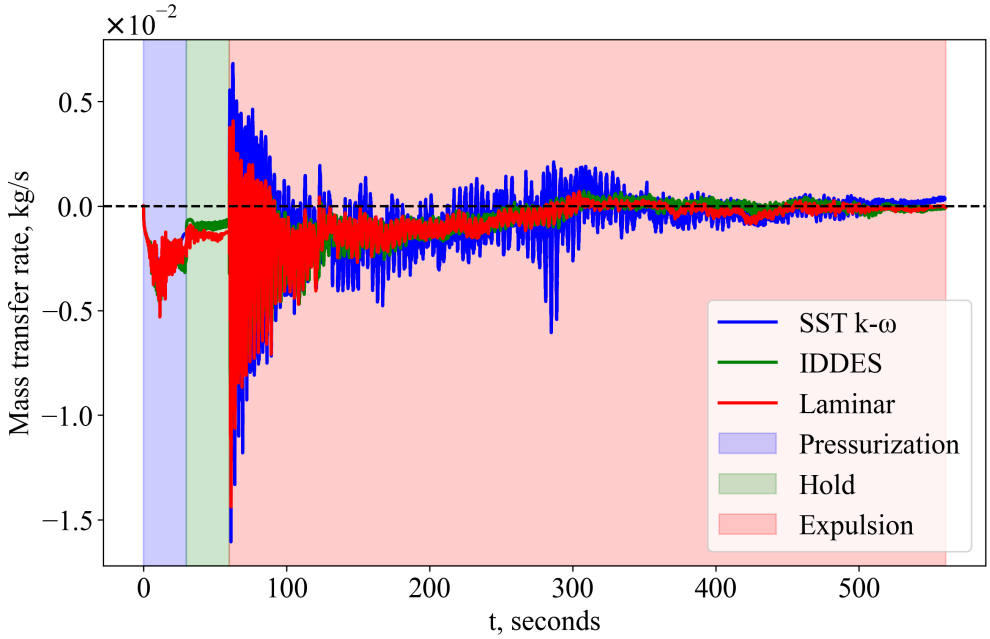

Fig. 4 CFD-predicted phase change rate in the tank during the test.

Figure 5 compares the added pressurant gas during expulsion for each turbulence model used alongside experimental data. Initially, the CFD predictions closely match the experimental measurements; however, as the expulsion process continues, the predictions diverge. Despite this divergence, the overall pressurant requirements predicted by the CFD models remain within 16% of the experimental values. This discrepancy can be attributed to uncertainties and assumptions made during the pressurization period. Since the tank conditions during expulsion depend on the initial and boundary conditions established during pressurization, any inaccuracies in modeling the initial stages can propagate. The slightly higher pressurant mass for the SST k-ω model can be attributed to its higher magnitudes of condensation

during the expulsion.

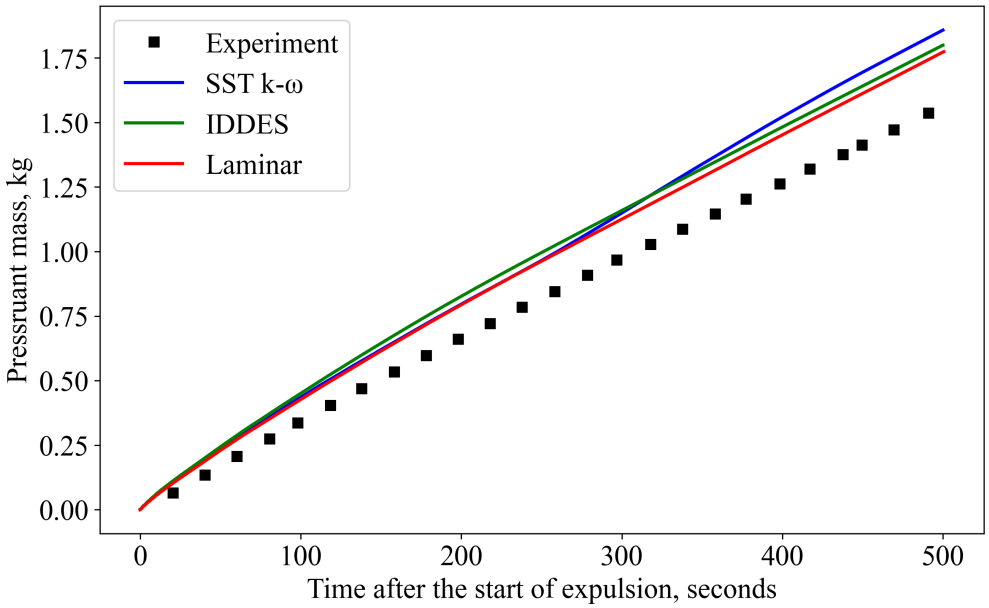

Fig. 5 Added pressurant gas during the expulsion.

Despite varying levels of complexity in the turbulence models, the laminar, SST k-ω, and IDDES models performed commendably in predicting the added pressurant mass during the expulsion. Surprisingly, the laminar model, which assumes smooth and orderly fluid motion without accounting for turbulence effects, yielded predictions aligning with experimental data. This indicates that, under the flow conditions present in the tank during expulsion, turbulent effects may be minimal or have a limited impact on the overall pressurant gas dynamics, allowing the laminar model to capture the essential behavior adequately.

The SST k-ω model predicts higher magnitudes of condensation and evaporation rates, resulting in slightly greater pressurant mass requirements. This suggests it more sensitively captures boundary layer effects and phase change processes at the vapor-liquid interface. As discussed in Section V.A, a damping factor is artificially applied in this model to control the level of turbulence generation at the interface. However, despite the application of the damping factor, the SST k-ω model may still overpredict turbulence in regions where the actual flow is relatively quiescent. This can lead to overestimating mass transfer rates due to enhanced mixing and heat transfer across the interface.

Consequently, the model predicts higher condensation rates, requiring more pressurant gas to maintain the tank pressure, as observed in the simulation results. The increased turbulence can also cause excessive thermal diffusion within the ullage, reducing the thermal stratification that is physically present under the given conditions. This results in a more uniform temperature distribution than experimental data, where thermal stratification is observed. These discrepancies highlight that while the SST k-ω model effectively captures certain interfacial phenomena, it may introduce artifacts that deviate from the actual behavior. Therefore, careful consideration and calibration are necessary when using this model to ensure accurate predictions of mass transfer, pressure evolution, and temperature distribution.

The IDDES model also provided predictions of the added pressurant mass that agreed with experimental measurements. Its capability to capture essential flow features and transient phenomena without high computational cost demonstrates its suitability for simulating unsteady and complex flow behaviors during expulsion. The IDDES model's dynamic adjustment of turbulence resolution allows it to naturally capture the appropriate turbulence scales influencing mass transfer and thermal fields. This leads to accurate predictions without artificial damping at the interface.

A mesh independence study was performed to confirm that the CFD results are unaffected by the computational mesh. Figure 6 presents the pressurant mass added during expulsion for the IDDES model, comparing results from the original, coarser, and finer meshes. The original mesh had an average cell size of 0.005 m; the coarse and fine meshes used average cell sizes of 0.01 m and 0.0025 m, respectively. Near-wall refinement was consistent across all three meshes, ensuring comparable resolution of boundary layer effects and gradients near the tank walls. The results showed that the added pressurant mass differed by less than 1% between the original, finer, and coarse meshes. This

minimal variation indicates that further mesh refinement does not significantly impact the solution. Additionally, the computational time increased substantially with the finer mesh without appreciable gains in accuracy. The findings indicate that the solution accurately reflects the physical behavior of the system, independent of mesh configuration.

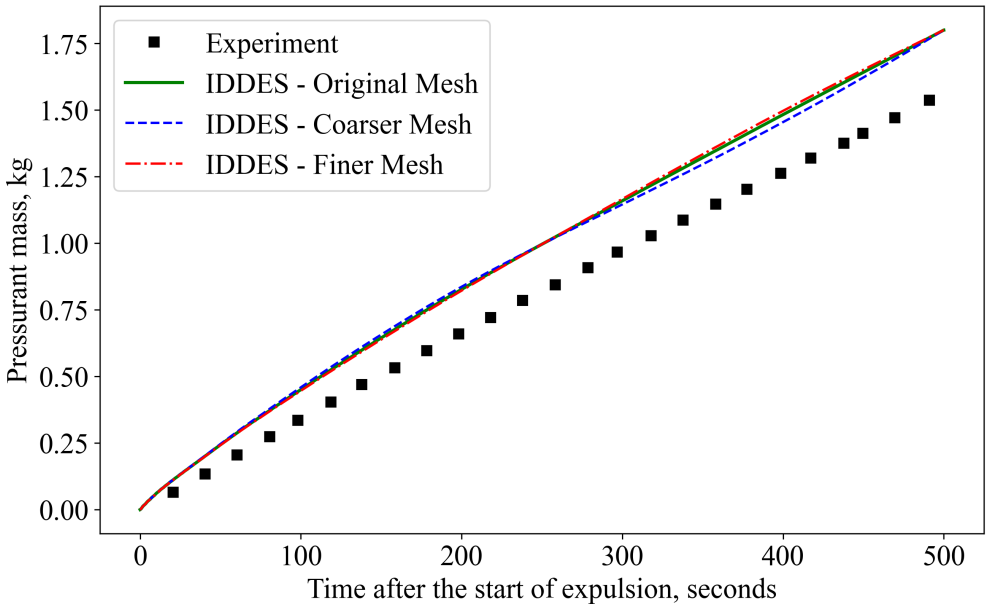

Fig. 6 Added pressurant gas during the expulsion for different meshes.

The experiment utilized thermocouples to measure the internal temperature distribution within and along the tank wall. These thermocouples were placed 0.24 meters from the tank's centerline, as shown in Figure 1b. To enable direct comparison, temperature monitors in the CFD model were positioned at the exact locations corresponding to the experimental thermocouples. Figures 7 and 8 present the temperature distributions inside the tank and along the tank wall, respectively, for both the CFD results and the experimental data near the end of the expulsion.

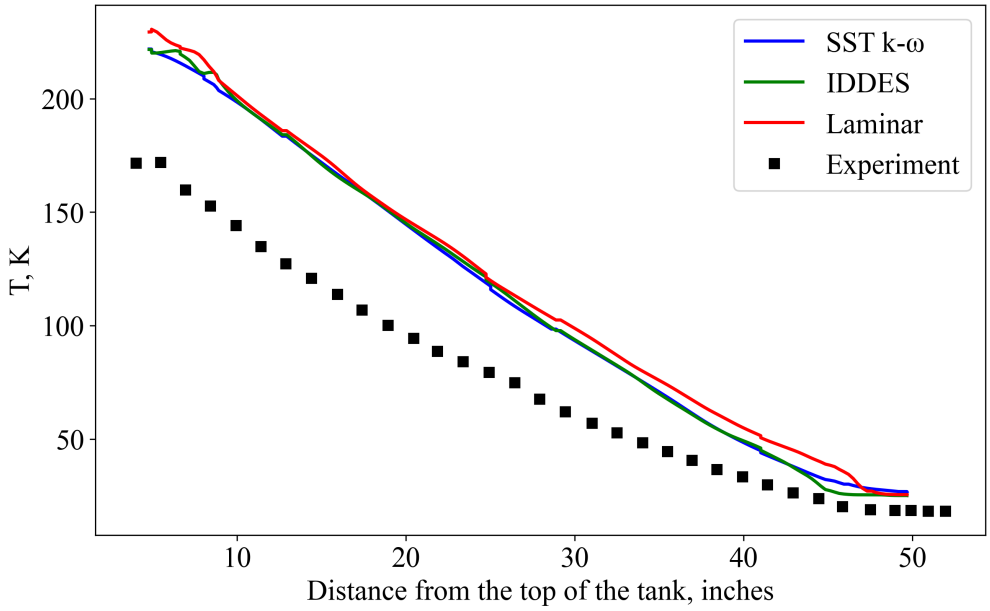

Fig. 7 Ullage temperature distribution in the tank near the end of the expulsion (t = 493 [s]) compared to experimental values.

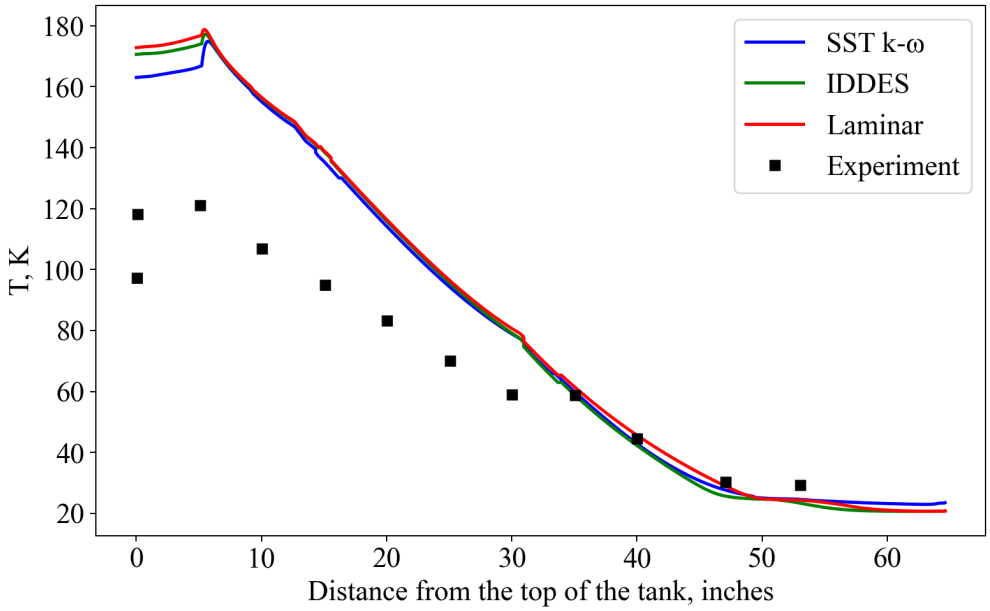

Fig. 8 Wall temperature distribution in the tank near the end of the expulsion (t = 493 [s]) compared to experimental values.

The CFD-predicted temperature distributions within the tank and along the tank wall follow the experimental trends but consistently overpredict the temperature values, particularly near the top of the tank. This overprediction is observed across all turbulence models used in the simulations. Notably, the discrepancy becomes more pronounced toward the tank's upper regions and diminishes toward the bottom, where the CFD results show good agreement with the experimental values.

The higher temperatures predicted by the CFD models can be attributed to several factors related to the assumptions

made during the pressurization and hold phases. Due to uncertainties and discrepancies in the experimental data during these phases, as discussed in Section V.D, a pressure inlet boundary condition was implemented in the CFD models to replicate the pressure ramp and maintain the target pressure during the hold phase. This approach may not fully capture the thermal and flow dynamics occurring in the tank during pressurization, such as the exact mass flow rates and temperatures of the incoming gas.

Furthermore, the CFD models assume a uniform and instantaneous distribution of the incoming pressurant gas, which may lead to overestimating heat transfer to the ullage region. Mixing the warmer pressurant gas with the cooler ullage gas is likely less efficient, resulting in lower temperatures than predicted.

Additionally, simplifications in modeling the pressurization process—such as neglecting the transient variations in inlet mass flow rate and temperature—can impact the tank's thermal history and lead to cumulative differences in temperature predictions during the expulsion phase. Since the initial thermal conditions at the start of expulsion are influenced by the preceding pressurization and hold periods, any inaccuracies in modeling these stages can propagate and amplify discrepancies in the temperature profiles.

Building upon the analysis of the temperature distributions within and along the tank wall, it is also instructive to examine the transient temperature behavior at specific locations within the ullage region. Figure 9 illustrates the temperature evolution during the expulsion phase at temperature monitor TP-34, located in the tank's upper ullage region. The CFD results at this location are plotted alongside the experimental temperature data for direct comparison. It can be observed that the CFD-predicted temperatures closely align with both the magnitude and trend of the experimental values. Specifically, the IDDES and laminar models show similar temperature increases and trends throughout the expulsion.

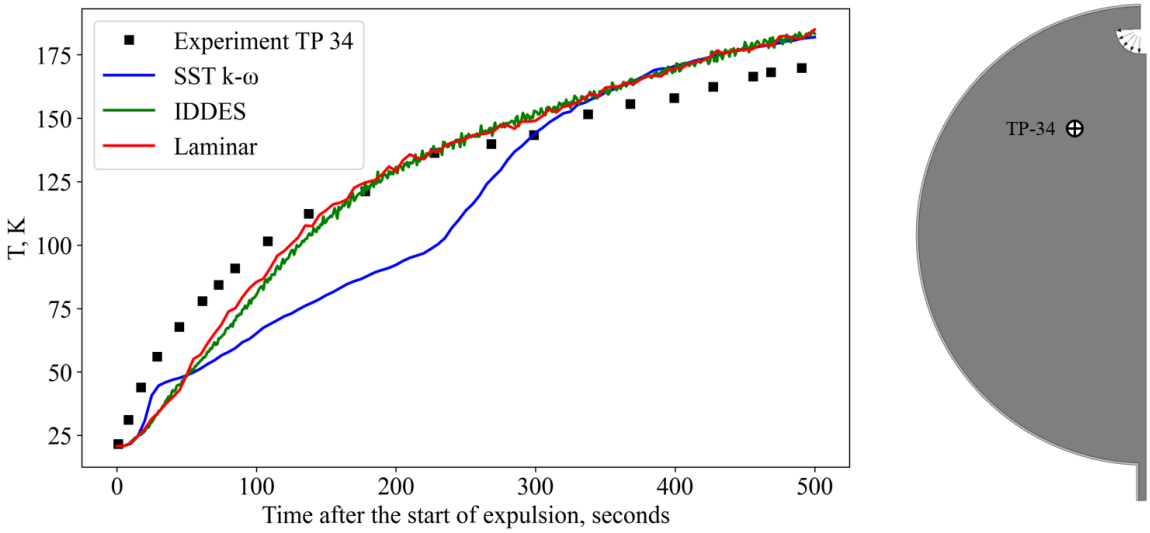

Fig. 9 Temperature evolution at temperature sensor TP-34.

In contrast, the SST k-ω model predicts a slower increase in temperature between 100 and 300 seconds into the expulsion phase. This discrepancy may stem from the model's tendency to predict higher TKE in certain flow conditions, resulting in increased thermal diffusion. The slower temperature rise suggests that the SST k-ω model spreads thermal energy more aggressively, dispersing it over a larger volume and transferring heat from the vapor region into the liquid region more rapidly than observed experimentally. This excessive thermal diffusion reduces the thermal stratification within the ullage, leading to a more uniform temperature distribution that deviates from the experimental observations.

On the other hand, the IDDES and laminar models preserve sharper thermal gradients closer to the experimental observations. As a result, both the IDDES and laminar models show a temperature increase at TP-34 that more closely matches the experimental data. The laminar model, lacking turbulence effects, maintains the natural stratification

expected under 1-g conditions. The IDDES model, with its dynamic adjustment of turbulence resolution, effectively captures the unsteady flow phenomena without introducing excessive turbulence at the interface.

Figures 10-12 present the temperature contours from the different turbulence models at the start and end of the expulsion phase. The white line marks the vapor-liquid interface. At the beginning of expulsion, the SST k-ω model shows a greater degree of temperature diffusion near the interface, with much of the vapor region from the interface to the inlet appearing warmer. In contrast, the laminar and IDDES models exhibit more pronounced temperature stratification in this region. Under 1-g conditions, the temperature in the tank should ideally be stratified; thus, the SST k-ω model introduces an artificial diffusion effect that does not occur in reality.

At the end of expulsion, all models display similar temperature contours, each with comparable levels of temperature stratification. This consistency aligns with the temperature distributions in the tank at the end of expulsion, as illustrated in Figures 7 and 8, where the model predictions closely match one another.

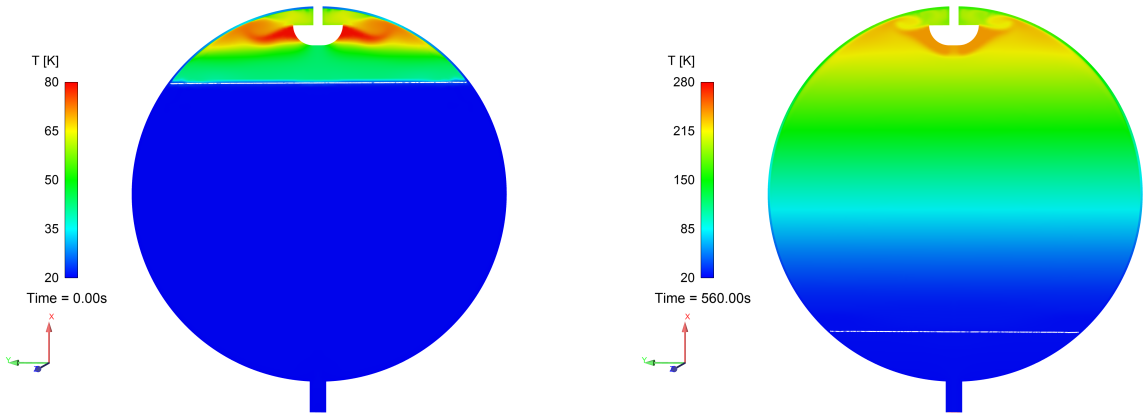

(a) SST k-ω, start of expulsion. **(b) SST k-ω, end of expulsion.**

Fig. 10 Temperature contours from the SST k-ω model at the start and end of expulsion.

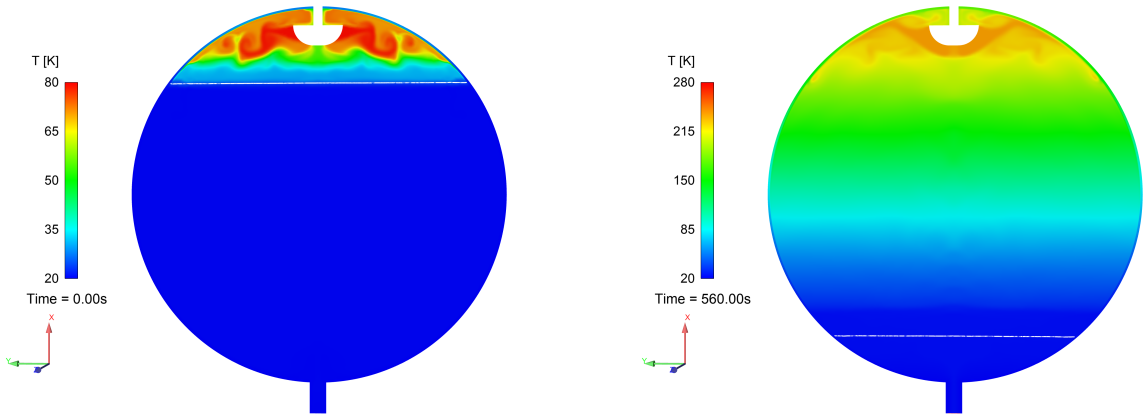

(a) Laminar, start of expulsion. **(b) Laminar, end of expulsion.**

Fig. 11 Temperature contours from the laminar model at the start and end of expulsion.

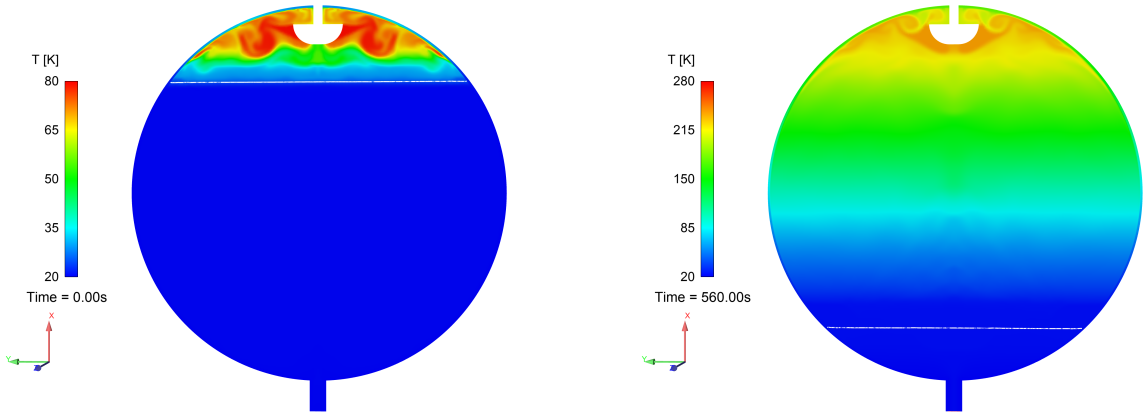

(a) IDDES, start of expulsion. **(b) IDDES, end of expulsion.**

Fig. 12 Temperature contours from the IDDES model at the start and end of expulsion.

VII. Conclusion

A computational model of K-site autogenous tank pressurization and expulsion of liquid hydrogen was developed. Its predictions were then compared with experimental data. This study utilized an in-house-developed VOF phase-change model to predict heat and mass transfer at the vapor-liquid interface.

Because discrepancies exist between the reported experimental pressurant use and the CFD results, we suspect some errors in the experimental pressurant mass measurements during the pressurization and hold phases. To address this issue, an inlet-pressure boundary condition was applied to match the linear pressure rise during tank pressurization. This approach also helped maintain the pressure at the target level during the hold stage. Inlet pressure, ullage volume, inlet temperatures, and the outlet mass flow rate were set to experimental values.

The CFD simulations were conducted using a laminar flow model and two turbulence models: SST k-ω and IDDES. Comparing these models allowed assessing their influence on fluid dynamics and heat transfer accuracy. The results agreed well with the experimental data for the tank pressure evolution and the pressurant mass added during expulsion across all models. The CFD model's predicted pressurant requirements were within 16% of the experimental measurements, regardless of the turbulence model used. Additionally, a mesh independence study verified that the computational results were unaffected by mesh density, reinforcing the reliability of the numerical solutions.

The CFD simulations predicted tank temperature distributions inside the tank and along the tank wall, which generally followed the experimental trends. However, they overpredicted the temperature values, particularly near the top of the tank at the end of the expulsion. This overprediction was observed across all turbulence models used. However, the models successfully captured the transient evolution of temperatures within the tank as the changes in CFD-predicted temperatures matched well with those observed in the experiment.

This study highlights the importance of selecting appropriate turbulence models to accurately simulate the flow and heat transfer phenomena during tank pressurization and expulsion. The comparison of laminar, SST k-ω, and IDDES turbulence models demonstrated that all models could predict the overall trends. However, differences in the predicted temperatures and phase-change rates were evident. The laminar and IDDES models better agreed with the experimental temperature evolution, whereas the SST k-ω model exhibited higher thermal diffusion.

Future work could involve refining the CFD model by incorporating more advanced turbulence models, such as an LES, or by adjusting thermal boundary conditions to improve temperature predictions. Such refinements may also be necessary due to uncertainties in the experimental measurements. Since these experiments were performed without prior consideration for CFD validation, specific data gaps exist, necessitating assumptions.

Overall, the validated CFD model, incorporating different turbulence models, provides a valuable tool for predicting the behavior of cryogenic propellant tanks during autogenous pressurization and expulsion. The insights gained from comparing different turbulence models improve the accuracy and reliability of CFD simulations, aiding in the design and analysis of such systems for future missions.

Acknowledgments

The authors thank the Modeling Portfolio Project within the STMD CFM Project Office for funding this work.

References

[1] Hardy, T. L., Whalen, M. V., Tomsik, T. M., Mahoney, N. B., and DeWitt, R. L., "Comparison of Pressurized Expulsion of Slush Hydrogen and Normal Boiling Point Liquid Hydrogen Using Hydrogen Pressurant Gas," Tech. rep., National Aerospace Plane (NASP) Technical Memorandum, 1991.

[2] Baker, M., Hauser, D., and Kartuzova, O., "CFD Modeling of a Cryogenic Methane Drain Test with and without Induced Sloshing," *30th Space Cryogenics Workshop*, 2023.

[3] Longmire, N., and Hauser, D., "Validation of Computational Fluid Dynamics Model for Pressurized Expulsion of Liquid Methane using Non-Condensable Pressurant," *Annual Thermal and Fluids Analysis Workshop (TFAWS)*, 2024.

[4] Kartuzova, O. V., Kassemi, M., and Hauser, D. M., "Validation of a Two-Phase CFD Model for Predicting Propellant Tank Pressurization and Pressure Collapse in The Ground-Based K-Site Hydrogen Slosh Experiment," *AIAA SCITECH 2024 Forum*, 2024, p. 0547.

[5] Hirt, C. W., and Nichols, B. D., "Volume of fluid (VOF) method for the dynamics of free boundaries," *Journal of computational physics*, Vol. 39, No. 1, 1981, pp. 201–225.

[6] Schrage, R. W., *A theoretical study of interphase mass transfer*, Columbia University Press, 1953.

[7] Brackbill, J. U., Kothe, D. B., and Zemach, C., "A continuum method for modeling surface tension," *Journal of computational physics*, Vol. 100, No. 2, 1992, pp. 335–354.

[8] *ANSYS Fluent User's Guide*, ANSYS, Inc., release 24.1 ed., 2023.

[9] Menter, F. R., "Two-equation eddy-viscosity turbulence models for engineering applications," *AIAA journal*, Vol. 32, No. 8, 1994, pp. 1598–1605.

[10] Shur, M. L., Spalart, P. R., Strelets, M. K., and Travin, A. K., "A hybrid RANS-LES approach with delayed-DES and wall-modelled LES capabilities," *International journal of heat and fluid flow*, Vol. 29, No. 6, 2008, pp. 1638–1649.

[11] Gritskevich, M. S., Garbaruk, A. V., Schütze, J., and Menter, F. R., "Development of DDES and IDDES formulations for the k-ω shear stress transport model," *Flow, turbulence and combustion*, Vol. 88, 2012, pp. 431–449.